


Determining non-Abelian topological order from infinite projected entangled pair statesAnna Francuz¹* and Jacek Dziarmaga*Institute of Theoretical Physics, Jagiellonian University, ul. Łojasiewicza 11, PL-30-348 Kraków, Poland* (Received 24 August 2020; revised 16 November 2020; accepted 17 November 2020; published 4 December 2020)

We generalize the method introduced in *Phys. Rev. B* **101**, 041108 (2020) of extracting information about topological order from the ground state of a strongly correlated two-dimensional system represented by an infinite projected entangled pair state (iPEPS) to non-Abelian topological order. When wrapped on a torus the unique iPEPS becomes a superposition of degenerate and locally indistinguishable ground states. We find numerical symmetries of the iPEPS, represented by infinite matrix product operators (MPO) and their fusion rules. The rules tell us how to combine the symmetries into projectors onto states with well defined anyon flux. A linear structure of the MPO projectors allows for efficient determination for each state its second Renyi topological entanglement entropy on an infinitely long cylinder directly in the limit of infinite cylinder's width. The same projectors are used to compute topological S and T matrices encoding mutual and self-statistics of emergent anyons. The algorithm is illustrated by examples of Fibonacci and Ising non-Abelian string net models.

DOI: [10.1103/PhysRevB.102.235112](https://doi.org/10.1103/PhysRevB.102.235112)**I. INTRODUCTION**

Topologically ordered phases [1] support anyonic quasiparticles. They open the possibility of realizing fault-tolerant quantum computation [2] based on braiding of non-Abelian anyons. Apart from a number of exactly solvable models [2–4], verifying whether a given microscopic Hamiltonian realizes a topologically ordered phase has traditionally been regarded as an extremely hard task. Recently, observation of quantized Hall effect in Kitaev-like ruthenium chloride α - RuCl_3 in magnetic field [5] granted the problem with urgent experimental relevance.

A leading numerical method is to use density matrix renormalization group (DMRG) [6,7] on a long cylinder [8–23]. In the limit of infinitely long cylinders, DMRG naturally produces ground states with well-defined anyonic flux, from which one can obtain full characterization of a topological order, via so-called topological S and T matrices [24]. Since the proposal of Ref. [24], this approach has become a common practice [25–42].

Unfortunately, the cost of a DMRG simulation grows exponentially with the circumference of cylinder, limiting this approach to thin cylinders (up to a width of $\simeq 14$ sites) and short correlation lengths (up to 1–2 sites). Instead, infinite projected entangled pair states (iPEPS) in principle allow for much longer correlation lengths [43–45]. A unique ground state on an infinite lattice can be represented by an iPEPS that is either a variational ansatz [46] or a result of numerical optimization [47,48]. When wrapped on a cylinder the iPEPS becomes a superposition of degenerate ground states with definite anyonic fluxes. Here we generalize the approach of Ref. [48] to non-Abelian topological order and show how to produce a PEPS-like tensor network for each ground state

with well-defined flux. Such tensor networks are suitable for extracting topological S and T matrices by computing overlaps between ground states. Furthermore, we show that they allow for computation of topological second Renyi entropy directly in the limit of infinite cylinder's width. The approach of Ref. [48] does not assume clean realization of certain symmetries on the bond indices, in contrast to Refs. [49–52]. This has been demonstrated in Ref. [48] by examples of toric code and double semions perturbed away from a fixed point towards a ferromagnetic phase as well as for the numerical iPEPS representing the ground state of the Kitaev model in the gapped phase. The last example shows that the method does not require restoring the symmetries by suitable gauge transformations of a numerical iPEPS, a feat that was accomplished in Ref. [53] for the toric code with a perturbation. Finally, it also has much lower cost than methods based on the tensor renormalization group [54].

The ferromagnetic Kitaev model in a weak (1,1,1) magnetic field supports non-Abelian chiral topological order [3,23] and Ref. [5] is believed to provide the first experimental realization of this universality class. However, as the magnetic field is a tiny perturbation of a critical state, the correlation length should be long [46]. This drives the problem beyond accurate DMRG simulation on a thin cylinder and, therefore, the non-Abelian phase observed in the experiment [5] may require iPEPS for its accurate description.

In this work we consider mainly string-net models. The key elements of the method introduced in Ref. [48] are shown in Fig. 1. Virtual indices of iPEPS on a torus or cylinder can be inserted with horizontal/vertical matrix product operator (MPO) symmetries. Their action on iPEPS is the same as flux operators (Wilson loops) winding around the torus in the same horizontal/vertical direction. However, the MPO symmetries are much easier to find than the nonlocal operators that—in interacting systems—become complicated operator ribbons rather than simple strings. Just as projectors on definite anyon

*Corresponding author: anna.francuz@uj.edu.pl

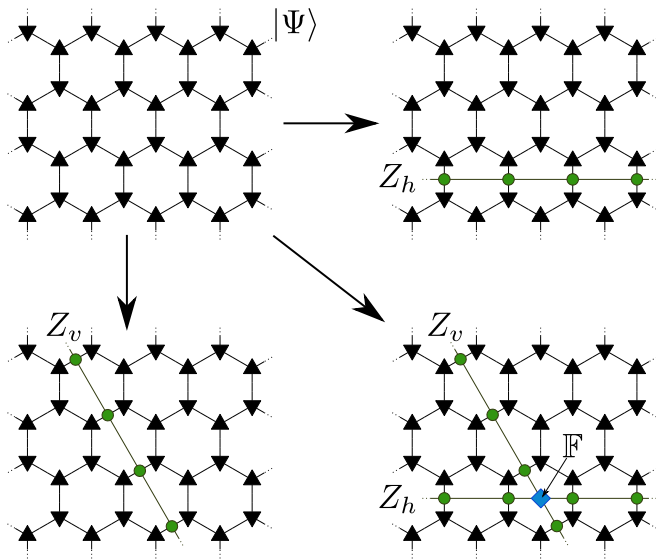


FIG. 1. General picture. From the unique ground state on an infinite lattice represented by an iPEPS $|\Psi\rangle$, we construct various states inserted with MPO symmetries. Their linear combinations, whose coefficients are determined by fusion rules of the MPO symmetries $Z_{h,v}$ (corresponding to anyonic fusion rules), become a basis of states with well defined anyonic flux. Here physical indices are not drawn for simplicity.

fluxes could be in principle constructed as linear combinations of flux operators, virtual projectors can be made as combinations of the MPO symmetries.

The paper is organized in Secs. II–VIII where we gradually introduce subsequent elements of the algorithm. Most sections open with a general part introducing a new concept. Then a series of subsections follows illustrating the general concept with a series of examples: the Abelian toric code (to make contact with Ref. [48]), Fibonacci string net, and Ising string net. In the end the algorithm is summarized in Sec. IX. Additionally, in Appendix E we apply some of the same tools to a variational ansatz proposed for the Kitaev model in magnetic field [46]. A detailed plan is as follows.

In Sec. II we define fixed points of the iPEPS transfer matrix in the form of MPS and introduce MPO symmetries that map between different fixed points. We also identify fusion rules of the MPO symmetries that are isomorphic with anyonic fusion rules. In Sec. III we consider an iPEPS wrapped on an infinite cylinder—that we visualize as horizontal without loss of generality—and use the fusion rules to construct vertical projectors on states with definite anyon flux along the horizontal cylinder. In Sec. IV we consider again an iPEPS wrapped on an infinite cylinder but this time the iPEPS is inserted with a horizontal MPO symmetry that alters boundary conditions in the vertical direction. We construct its vertical MPO symmetries that we call impurity MPO (IMPO) symmetries. We also identify their fusion rules. In Sec. V the fusion rules are used to construct vertical projectors as linear combinations of the IMPO symmetries. The impurity projectors select states with definite horizontal anyon flux in the iPEPS inserted with the horizontal MPO symmetry. In Sec. VI we show how the structure of vertical projectors enables efficient evaluation of

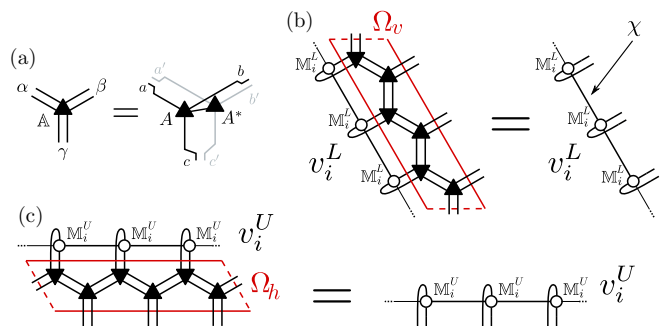


FIG. 2. Transfer matrix. In (a), graphical representation of a double tensor \mathbb{A} . In (b), leading left eigenvector $(v_i^L|)$ of vertical transfer matrix Ω_v takes an MPO form v_i^L . The uniform v_i^L is made of tensors \mathbb{M}_i^L with bond dimension χ that can be obtained with the VUMPS algorithm [55,56]. In (c), up eigenvector v_i^U of horizontal TM Ω_h .

the topological second Renyi entanglement entropy directly in the limit of infinite cylinder's width. In Sec. VII the same is done with impurity projectors. Finally, in Sec. VIII we show how to obtain the topological S and T matrices from overlaps between states with definite anyon flux. In the case of string net models they provide full characterization of the topological order. The paper is closed with a brief summary in Sec. IX.

II. GENERATORS OF SYMMETRIES

Uniform iPEPS on a honeycomb lattice can be characterized by a tensor A with elements A_{abc}^i . Here, i is a physical index and a, b, c are bond indices. Let \mathbb{A} denote a double tensor $\mathbb{A} = \sum_i A^i \otimes (A^i)^*$ with double bond indices $\alpha = (a, a')$, etc., see Fig. 2(a) and Appendix B. iPEPS transfer matrix (TM) Ω is defined by a line of double tensors \mathbb{A} contracted via their bond indices along the line as shown in Figs. 2(b) and 2(c). These figures show vertical TM Ω^v and horizontal TM Ω^h , respectively. Their leading eigenvectors are TM fixed points. In the thermodynamic limit only the leading eigenvectors survive in TM's spectral decomposition:

$$\bar{\Omega}^v \approx \omega \sum_{i=1}^n |v_i^R\rangle \langle v_i^L|, \quad \bar{\Omega}^h \approx \omega \sum_{i=1}^n |v_i^U\rangle \langle v_i^D|. \quad (1)$$

The leading eigenvalue ω is the same for both vertical and horizontal TM. The leading eigenvectors are biorthonormal:

$$\delta_{ij} = (v_i^L|v_j^R) = \text{Tr} (v_i^L)^T v_j^R, \quad (2)$$

$$\delta_{ij} = (v_i^U|v_j^D) = \text{Tr} (v_i^U)^T v_j^D. \quad (3)$$

Here we use both the MPS $|v_i\rangle$ and MPO v_i forms. MPS $|v_i\rangle$ is MPO v_i between bra and ket indices of the double iPEPS TM. The ansatz for a fixed point boundary v_i^X is a pure MPO with spectral radius 1 [57] made out of tensors M_i^X .

Different fixed points are connected by symmetries whose existence is a distinctive feature of topologically ordered states encoded in iPEPS. In contrast, in the trivial ferromagnetic phase the two boundary fixed points, v_\uparrow and v_\downarrow , corresponding to two different magnetizations have orthogonal spaces and, therefore, the operator mapping

between them does not exist. The symmetries act on virtual indices of the tensor network. They are called MPO symmetries and, apart from a few exactly solvable models for which they can be found analytically [49], they have to be found numerically as described in Ref. [48]. The MPO symmetries Z_a are operators which form certain algebra under their multiplication:

$$Z_a Z_b = \sum_c N_{ab}^c Z_c, \quad (4)$$

where the possible values of N_{ab}^c are 0,1. Each MPO symmetry Z_a (including the trivial identity $Z_1 \equiv 1$) corresponds to a certain anyon type a in a sense that their algebra is the same as the fusion rules of the anyons, see Appendix A. Once all boundary fixed points v_i are found numerically, the MPO symmetries z_{ij} are obtained as MPO's mapping between the boundaries:

$$v_i \cdot z_{ij} = v_j. \quad (5)$$

The same set of symmetries exists for L/R and U/D boundary fixed points. We completed these numerical procedures in the following models.

A. Toric code

We begin with this basic example to make contact with Ref. [48] where the Abelian version of the present method was applied to this model and its realistic implementation with the Kitaev model [3]. Each TM has two boundary fixed points. To be more specific, for vertical transfer matrix Ω^v in addition to $Z_1^v = 1$ we find numerically one nontrivial MPO symmetry $z_{12}^v = z_{21}^v \equiv Z_2^v$ that satisfies

$$v_1^L \cdot Z_2^v = v_2^L, \quad v_2^L \cdot Z_2^v = v_1^L. \quad (6)$$

These equations imply Z_2 algebra:

$$Z_2^v \cdot Z_2^v = 1. \quad (7)$$

It has to be strongly emphasized that in general the numerical solution Z_2^v of equation (6) has zero modes that make the algebra valid only in the sense that $v_i^L \cdot Z_2 \cdot Z_2 = v_i^L$ for any i . The same reservation applies to all fusion rules (4) to be identified numerically in the rest of this paper. This is also why all (numerically obtained) MPO symmetries throughout the paper are used only in iPEPS embedding: The zero modes do not matter when inserted between columns/rows of an iPEPS. Keeping this in mind, for all fixed point tensors considered in this paper the algebra (4) is satisfied with close to machine precision.

B. Fibonacci string net

Here we employed the iPEPS tensors for a fixed point Fibonacci string net model presented in Appendix B. For each TM we found numerically two boundary fixed points and one nontrivial MPO symmetry Z_2 satisfying, e.g.,

$$v_1^L \cdot Z_2^v = v_2^L. \quad (8)$$

The same MPO was found to satisfy also

$$v_2^L \cdot Z_2^v = v_1^L + v_2^L. \quad (9)$$

These two equations imply the Fibonacci fusion rule

$$Z_2^v \cdot Z_2^v = 1^v + Z_2^v. \quad (10)$$

Again, due to zero modes, the rule holds only when applied to iPEPS boundaries. Similar MPO symmetries were also found for the horizontal boundary fixed points.

C. Ising string net

Here we employed the iPEPS tensors for a fixed point Ising string net model presented in Appendix B. This time each TM has three boundary fixed points. We found two nontrivial MPO symmetries, labeled as Z_σ and Z_ψ , as numerical solutions to equations, e.g.,

$$v_1^L \cdot Z_\sigma^v = v_2^L, \quad v_1^L \cdot Z_\psi^v = v_3^L. \quad (11)$$

Furthermore, we found that the solutions satisfy

$$\begin{aligned} v_2^L \cdot Z_\sigma^v &= v_1^L + v_3^L, & v_3^L \cdot Z_\psi^v &= v_1^L, \\ v_2^L \cdot Z_\psi^v &= v_2^L, & v_3^L \cdot Z_\sigma^v &= v_2^L. \end{aligned} \quad (12)$$

These six equations imply nontrivial fusion rules:

$$\begin{aligned} Z_\sigma^v \cdot Z_\sigma^v &= 1^v + Z_\psi^v, \\ Z_\sigma^v \cdot Z_\psi^v &= Z_\sigma^v = Z_\psi^v \cdot Z_\sigma^v, \\ Z_\psi^v \cdot Z_\psi^v &= 1^v, \end{aligned} \quad (13)$$

which justify the labeling. For our numerical Z_ψ^v and Z_σ^v the rules hold only when applied to v_i^L . Similar MPO symmetries were also found for the horizontal boundary fixed points.

III. VERTICAL PROJECTORS

The MPO symmetries alone are enough to construct some of the projectors on states with definite anyon fluxes. Let us consider vertical MPO symmetries Z_a^v for definiteness. Their linear combinations

$$P = \sum_a c_a Z_a^v, \quad (14)$$

which satisfy $P \cdot P = P$, make vertical projectors. When these projectors are inserted into iPEPS wrapped on an infinite horizontal cylinder, they yield states with definite anyon fluxes along that cylinder. The remaining projectors that can be applied when the iPEPS is inserted with a line of Z^h are the subject of the following section.

A. Toric code

The Z_2 algebra (7) allows for two projectors,

$$P_\pm = \frac{1}{2}(1 \pm Z_2^v), \quad (15)$$

that satisfy $P_\pm \cdot P_\pm = P_\pm$ and $P_+ \cdot P_- = 0 = P_- \cdot P_+$. Later on they will be identified as $P_+ \equiv P_{\text{vac}}$ and $P_- \equiv P_e$, i.e., projectors on the vacuum and the electric flux, respectively.

B. Fibonacci string net

The fusion rules (10) determine two projectors:

$$P_\pm = \frac{1}{\sqrt{5}}(\phi^{\pm 1} 1 \mp Z_2^v). \quad (16)$$

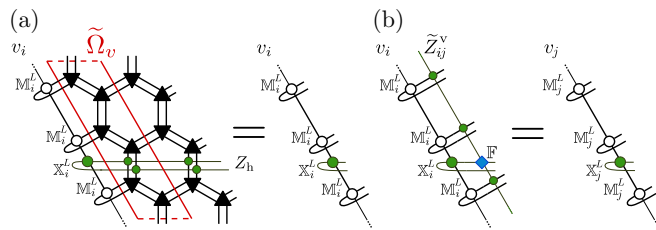


FIG. 3. Impurity transfer matrix. In (a), with Z^h inserted into both bra and ket layers of the iPEPS the transfer matrix Ω^v becomes impurity transfer matrix $\tilde{\Omega}^v$. Its leading left eigenvectors ($x^L|$) are obtained from MPOs from v^L by inserting additional tensors \mathbb{X}^L . Here double lines are dropped to improve clarity. In (b), graphical illustration of Eq. (22).

Here $\phi = (\sqrt{5} + 1)/2$. They will be identified as $P_+ \equiv P_{\text{vac}}$ and $P_- \equiv P_{\tau\bar{\tau}}$, i.e., projectors on the vacuum and the sector with both Fibonacci anyons: τ and $\bar{\tau}$.

C. Ising string net

The fusion rules (13) allow for six projectors:

$$P_{1,2} = \frac{1}{2}(1^v \pm Z_\psi^v), \quad (17)$$

$$P_{3,4} = \frac{1}{4}(31^v - Z_\psi^v) \pm \frac{1}{\sqrt{8}}Z_\sigma^v, \quad (18)$$

$$P_{5,6} = \frac{1}{4}(1^v + Z_\psi^v) \pm \frac{1}{\sqrt{8}}Z_\sigma^v. \quad (19)$$

Not all of them are the minimal projectors on definite anyon flux. It is easy to check that $P_3 \cdot P_4 = P_2$ and, therefore, out of the three it is enough to keep only P_2 . Furthermore, we can see that $P_5 + P_6 = P_1$ hence we can skip P_1 . After this selection we are left with three minimal projectors $P_{2,5,6}$ that satisfy $P_a \cdot P_b = P_a \delta_{ab}$. They will be identified as $P_5 \equiv P_{\text{vac}}$, $P_6 \equiv P_{\psi\bar{\psi}}$, and $P_2 \equiv P_{\sigma\bar{\sigma}}$.

IV. IMPURITY MPO SYMMETRIES

In order to construct the remaining projectors that are to be applied to an iPEPS inserted with a nontrivial horizontal MPO symmetry Z^h , we need to introduce an impurity transfer matrix (ITM), see Fig. 3(a). In general ITM has a number of leading left and right eigenvectors, respectively ($x_i^L|$ and $|x_j^R\rangle$), that are biorthonormal: $(x_i^L|x_j^R) = \delta_{ij}$. The eigenvectors are constructed by inserting the eigenvectors of the vertical TM, respectively v^L and v^R , with additional tensors \mathbb{X}_i^L and \mathbb{X}_j^R , see Fig. 3(a). The same figure shows equations that need to be satisfied by the additional tensors. They are efficiently obtained from a generalized eigenvalue problem:

$$(x_i^L|\tilde{\Omega}_v|x_j^R) = \lambda(x_i^L|x_j^R). \quad (20)$$

Here $\lambda = 1$ is the maximal generalized eigenvalue. The problem is to be understood as

$$(\mathbb{X}_i^L)^T \cdot \mathcal{M} \cdot \mathbb{X}_j^R = \lambda(\mathbb{X}_i^L)^T \cdot \mathcal{N} \cdot \mathbb{X}_j^R, \quad (21)$$

where \mathbb{X}_i^L and \mathbb{X}_j^R are vectorized and matrices \mathcal{M} and \mathcal{N} are tensor environments of \mathbb{X}_i^L and \mathbb{X}_j^R in $(x_i^L|\tilde{\Omega}_v|x_j^R)$ and $(x_i^L|x_j^R)$, respectively.

Furthermore, as shown in Fig. 3(b), the left eigenvector ($x_i^L|$) can be acted on by any vertical MPO symmetry Z^v , including the trivial identity $Z_1^v = 1^v$. In order to make the action possible, Z^v has to be inserted with additional tensor \mathbb{F} that acts on Z^h . With the appropriate choice of \mathbb{F}_{ij} their combination gives rise to impurity MPO-symmetry \tilde{z}_{ij}^v such that

$$x_i^L \tilde{z}_{ij} = x_j^L. \quad (22)$$

A necessary condition for symmetry \tilde{z}_{ij}^v to exist is that v^L in x_i^L , here denoted by $v^L(i)$, and v^L in x_j^L , here denoted by $v^L(j)$, are related by $v^L(i) \cdot Z^v = v^L(j)$.

A straightforward but essential observation is that, in analogy to MPO symmetries, the IMPO symmetries also satisfy their own fusion rules:

$$\tilde{Z}_a^v \cdot \tilde{Z}_b^v = \sum_c \tilde{N}_{ab}^c \tilde{Z}_c^v. \quad (23)$$

Here we keep only the minimal set of independent IMPO symmetries denoted by a capital \tilde{Z} and labeled with a single index a, b, c . In general the coefficients \tilde{N}_{ab}^c do not need to be integers as they depend on normalization of the eigenvectors ($x_i^L|$ and $|x_j^R\rangle$).

V. IMPURITY PROJECTORS

In analogy to the vertical MPO symmetries and vertical projectors, as a product of two IMPO symmetries is a linear combination of IMPO symmetries, see Eq. (23), we can find projectors as linear combinations of IMPO symmetries,

$$\tilde{P} = \sum_a \tilde{c}_a \tilde{Z}_a^v. \quad (24)$$

The condition $\tilde{P} \cdot \tilde{P} = \tilde{P}$ is equivalent to a set of quadratic equations for coefficients \tilde{c}_a . Numerically it seems more efficient to find the coefficients by repeated Lanczos iterations:

$$\tilde{P}' \propto \tilde{P} \cdot \tilde{P}. \quad (25)$$

In each iteration the IMPO fusion rules (23) are used to express the product $\tilde{P} \cdot \tilde{P}$ as a new linear combination $\tilde{P}' = \sum_a \tilde{c}'_a \tilde{Z}_a^v$ and then new coefficients \tilde{c}'_a are normalized so that the maximal magnitude of the eigenvalues of \tilde{P}' is 1. Therefore, each iteration is a map $\{c_a\} \rightarrow \{c'_a\}$ which is repeated until the coefficients converge. These computations are performed in the biorthonormal eigenbasis of impurity eigenvectors, ($x_a^L|$ and $|x_a^R\rangle$), where all involved MPO's become small matrices like, e.g., $(x_a^L|\tilde{Z}_c^v|x_b^R) \equiv [Z_c^v]_{ab}$. Repeating the Lanczos scheme with random initial coefficients we obtain all impurity projectors.

A. Toric code

There is one ITM with $Z^h = Z_2^h$. It has two eigenvectors ($x_a^L|$), one for each TM eigenvector v_a^L . In addition to an identity, $\tilde{1}^v$, there is one nontrivial IMPO symmetry $\tilde{z}_{12}^v = \tilde{z}_{21}^v \equiv \tilde{Z}_2^v$. A nontrivial fusion \mathcal{Z}_2 algebra, $\tilde{Z}^v \cdot \tilde{Z}^v = 1^v$, implies two projectors:

$$\tilde{P}_\pm = \frac{1}{2}(\tilde{1}^v \pm \tilde{Z}_2^v). \quad (26)$$

They will be identified as magnetic and fermionic projectors, $\tilde{P}_+ \equiv \tilde{P}_m$ and $\tilde{P}_- \equiv \tilde{P}_e$, respectively.

B. Fibonacci string net

There is one ITM with $Z^h = Z_2^h$. It has one eigenvector (x_1^L embedded in v_1^L and two eigenvectors ($x_{2,3}^L$ embedded in v_2^L). We choose the two to be Hermitian and orthonormal but this still leaves (gauge) freedom of their rotation. In addition to the trivial identity, $\hat{1}^v$, there are two ITM symmetries: \tilde{z}_{12}^v and \tilde{z}_{13}^v . Their fusion rules do depend on the gauge but independently of the gauge we find numerically three projectors $P_{1,2,3}$. Only two of them project on states that are orthogonal to the states obtained with vertical projectors, as can be verified by calculating overlaps between their respective projected iPEPS on infinite torus. The new projectors will be identified as $\tilde{P}_1 \equiv \tilde{P}_\tau$ and $\tilde{P}_2 \equiv \tilde{P}_{\bar{\tau}}$.

Interestingly, the third one, \tilde{P}_3 , projects on the same horizontal anyon flux as vertical projector P_- and both will be identified as $\tilde{P}_{\tau\bar{\tau}}$ and $P_{\tau\bar{\tau}}$, respectively. This way we have two equivalent ways to obtain $\tau\bar{\tau}$ flux: one with and one without inserted Z_2^h MPO symmetry. In other words, with or without inserted Z_2^h symmetry the iPEPS wrapped on an infinite cylinder has a nonzero overlap with the ground state with $\tau\bar{\tau}$ flux.

C. Ising string net

There are two ITM with Z_σ^h and Z_ψ^h . For each of them independently we construct impurity projectors. In case of Z_σ^h we find four projectors to be identified later as \tilde{P}_σ , $\tilde{P}_{\bar{\sigma}}$, $\tilde{P}_{\sigma\bar{\psi}}$, and $\tilde{P}_{\psi\bar{\sigma}}$. In the case of Z_ψ^h we find three projectors to be identified as \tilde{P}_ψ , $\tilde{P}_{\bar{\psi}}$, and $\tilde{P}_{\sigma\bar{\sigma}}$. The last one provides a new way to obtain $\sigma\bar{\sigma}$ flux in addition to vertical projector $P_2 \equiv P_{\sigma\bar{\sigma}}$. This is similar redundancy as in the Fibonacci model.

VI. TOPOLOGICAL ENTROPY: VERTICAL PROJECTORS

The topological entanglement entropy (TEE) [58] is not full characterization of topological order but it may provide quick and numerically stable diagnostic for an iPEPS obtained by numerical minimization. Studies of von Neumann TEE of PEPS wave functions have long tradition [59] but they require finding full entanglement spectrum of an infinite half-cylinder and extrapolation to the limit of its infinite width, a task that may be hard to accomplish for a long correlation length. In contrast, the projector formalism is naturally compatible with the second Renyi entropy allowing for its efficient evaluation directly in the thermodynamic limit. What is more, in the realm of string net models the Renyi and von Neumann TEE were shown to be the same [60].

Here we consider a vertical cut in an iPEPS wrapped on an infinite horizontal cylinder of width L_v . Its right/left boundary fixed point on the left/right half-cylinder is σ_L/σ_R . A reduced density matrix for a half cylinder is isomorphic to [59]

$$\rho \propto \sqrt{\sigma_L^T} \sigma_R \sqrt{\sigma_L^T} \quad (27)$$

and its second Renyi entropy is

$$S_2 = -\log \text{Tr} \rho^2 = -\log \text{Tr} \sigma_L^T \sigma_R \sigma_L^T \sigma_R. \quad (28)$$

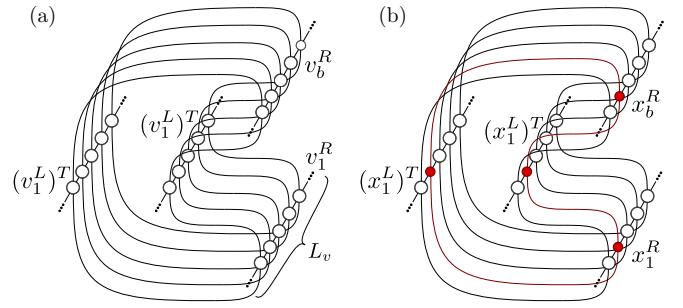


FIG. 4. Topological entropy. In (a), tensor network representing $(v_1^L)^T v_1^R (v_1^L)^T v_b^R$ on a vertical cut in an infinite horizontal cylinder of vertical width L_v . The network is L_v th power of a transfer matrix. In (b), tensor network representing $(x_1^L)^T x_1^R (x_1^L)^T x_b^R$. The network is L_v th power of the same transfer matrix inserted with a layer of impurities $\mathbb{X}_b^{L,R}$.

We want the entropy in a state with a definite anyon flux a along the cylinder.

Towards this end, we begin with $\sigma_{L,R} \propto v_1^{L,R}$ that is a combination of all anyon fluxes. After inserting projector P_a into the vertical cut we obtain

$$\rho_a = \mathcal{N}_a \sqrt{(v_1^L)^T} (v_1^R \cdot P_a^T) \sqrt{(v_1^L)^T}. \quad (29)$$

Here the projector was applied to $\sigma_R \propto v_1^R$ without loss of generality and normalization \mathcal{N}_a is such that $\text{Tr} \rho_a = 1$. The entropy becomes

$$\begin{aligned} S_2(a) &= -\log \text{Tr} \rho_a^2 \\ &= -\log \mathcal{N}_a^2 \text{Tr} (v_1^L)^T (v_1^R \cdot P_a^T) (v_1^L)^T (v_1^R \cdot P_a^T) \\ &= -\log \mathcal{N}_a^2 \text{Tr} (v_1^L)^T v_1^R (v_1^L)^T P_a^* v_1^R \cdot P_a^T \\ &= -\log \mathcal{N}_a^2 \text{Tr} (v_1^L)^T v_1^R (v_1^L)^T v_1^R P_a^T P_a^T \\ &= -\log \mathcal{N}_a^2 \text{Tr} (v_1^L)^T v_1^R (v_1^L)^T (v_1^R \cdot P_a^T). \end{aligned} \quad (30)$$

Here we used $P_a^T (v_1^L)^T = (v_1^L)^T P_a^*$ and $P_a^* v_1^R = v_1^R P_a^T$ that follow from the fact that v 's are edges of a double-layer iPEPS with bra and ket layers. In this way we are left with only one projector that yields a linear combination,

$$v_1^R \cdot P_a^T = \sum_b s_b^a v_b^R, \quad (31)$$

with coefficients s_b^a that follow from the properties of the MPO symmetries whose linear combination is P_a .

The normalization $\text{Tr} \rho_a = 1$ and the biorthonormality, $\text{Tr} (v_1^L)^T v_b^R = \delta_{1b}$, fix $\mathcal{N}_a = 1/s_1^a$. The entropy becomes

$$S_2(a) = -\log \sum_b \frac{s_b^a}{(s_1^a)^2} \text{Tr} (v_1^L)^T v_1^R (v_1^L)^T v_b^R. \quad (32)$$

The trace is a tensor network in Fig. 4(a). It is equal to a trace of L_v th power of a transfer matrix. For large enough L_v the network becomes

$$\text{Tr} (v_1^L)^T v_1^R (v_1^L)^T v_b^R = G_b \Lambda_b^{L_v}. \quad (33)$$

Here Λ_b is the leading eigenvalue of the transfer matrix and G_b its degeneracy. For large enough L_v the entropy is dominated

by terms with the maximal leading eigenvalue,

$$\Lambda = \text{Max}_b \Lambda_b, \quad (34)$$

and becomes

$$S_2(a) = -\log \Lambda^{L_v} \sum_b \frac{G_b s_b^a}{(s_1^a)^2} \equiv \alpha L_v - \gamma_a. \quad (35)$$

Here the sum is restricted to indices b with $\Lambda_b = \Lambda$. The area law has a coefficient

$$\alpha = -\log \Lambda \quad (36)$$

that does not depend on anyon flux a and the TEE is

$$\gamma_a = \log \sum_b \frac{G_b s_b^a}{(s_1^a)^2}. \quad (37)$$

We evaluate this expression in several examples.

A. Toric code

The projector yields $v_{\pm}^R \cdot P_{\pm}^T = (v_1^R \pm v_2^R)/2$, hence $s_1^{\pm} = 1/2$ and $s_2^{\pm} = \pm 1/2$. Furthermore, we obtain $\text{Tr}(v_1^L)^T v_1^R (v_1^L)^T v_b^R = \Lambda^{L_v}$ when $b = 1$ and zero otherwise. There is no degeneracy, $G_1 = 1$. Therefore,

$$\gamma_{\pm} = \log \sum_b 4s_b^{\pm} = \log 4s_1^{\pm} = \log 2. \quad (38)$$

This number is consistent with the anticipated identification $P_+ \equiv P_{\text{vac}}$ and $P_- \equiv P_e$.

B. Fibonacci string net

The projector yields $v_{\pm}^R \cdot P_{\pm}^T = (\phi^{\pm 1} v_1^R \mp v_2^R)/\sqrt{5}$, hence $s_1^{\pm} = \phi^{\pm 1}/\sqrt{5}$ and $s_2^{\pm} = \mp 1/\sqrt{5}$. We obtain with numerical precision:

$$\gamma_+ = \log \mathcal{D}, \quad \gamma_- = \log \frac{\mathcal{D}}{d_{\tau} d_{\bar{\tau}}}, \quad (39)$$

where $\mathcal{D} = 2 + \phi$ is the total quantum dimension and $d_{\tau} = d_{\bar{\tau}} = \phi$. These numbers are consistent with the identification $P_+ \equiv P_{\text{vac}}$ and $P_- \equiv P_{\tau\bar{\tau}}$.

C. Ising string net

Following similar lines for the double Fibonacci string net we obtain

$$\gamma_5 = \log \mathcal{D}, \quad \gamma_6 = \log \frac{\mathcal{D}}{d_{\psi} d_{\bar{\psi}}}, \quad \gamma_2 = \log \frac{\mathcal{D}}{d_{\sigma} d_{\bar{\sigma}}} \quad (40)$$

with numerical precision. Here the total quantum dimension $\mathcal{D} = 4$, $d_{\sigma} = d_{\bar{\sigma}} = \sqrt{2}$, and $d_{\psi} = d_{\bar{\psi}} = 1$. They are consistent with the identifications: $P_5 \equiv P_{\text{vac}}$, $P_6 \equiv P_{\psi\bar{\psi}}$, and $P_2 \equiv P_{\sigma\bar{\sigma}}$.

VII. TOPOLOGICAL ENTROPY: IMPURITY PROJECTORS

For impurity projectors that act on an iPEPS that is inserted with Z^h calculation of entropy goes along similar lines but with modifications accounting for Z^h . Accordingly, we begin with $\sigma^{L,R} = x_1^{L,R}$. Here x_i^L and x_j^R are MPO forms of impurity eigenstates ($|x_i^L\rangle$ and $|x_j^R\rangle$), respectively. As usual, their

left/right indices correspond to the bra/ket layer. The action of \tilde{P}_a yields

$$x_1^R \cdot \tilde{P}_a^T = \sum_b \tilde{s}_b^a x_b^R. \quad (41)$$

Here coefficients \tilde{s}_b^a are real because x_b^R are Hermitian. Taking into account normalization that follows from their biorthonormality, $\delta_{i_1 i_2} = (x_{i_1}^L | x_{i_2}^R) = \text{Tr}(x_{i_1}^L)^T x_{i_2}^R$, the entropy in sector a becomes

$$S_2(a) = -\log \sum_b \frac{\tilde{s}_b^a}{(\tilde{s}_1^a)^2} \text{Tr}(x_1^L)^T x_1^R (x_1^L)^T x_b^R. \quad (42)$$

The trace is a trace of the tensor network in Fig. 4(b). It is a trace of L_v th power of a transfer matrix times a layer of impurities $\mathbb{X}_b^{L,R}$. The transfer matrix is the same as in Fig. 4(a). For large enough cylinder width L_v the sum is dominated by indices b such that $\Lambda_b = \Lambda$, where Λ is the same maximal leading eigenvalue of the transfer matrices:

$$S_2(a) = \alpha L_v - \tilde{\gamma}_a. \quad (43)$$

Here $\alpha = -\log \Lambda$ is the same as for vertical projectors and independent of anyon flux a . The topological entropy is

$$\tilde{\gamma}_a = \log \sum_b \frac{\tilde{s}_b^a}{(\tilde{s}_1^a)^2} \sum_{m=1}^{G_b} X_{b,m}^a. \quad (44)$$

Here

$$X_{b,m}^a = (U_{b,m} | \text{Tr}(\mathbb{X}_1^L)^T \mathbb{X}_1^R (\mathbb{X}_1^L)^T \mathbb{X}_1^R | D_{\{b\},m}) \quad (45)$$

is a form factor where $(U_{1,m} |$ and $|D_{1,m})$ are the up and down leading eigenvectors of the transfer matrix in Fig. 4(b), numbered by $m = 1 \dots G_b$ where G_b is the degeneracy of the leading eigenvalue, and $\text{Tr}(\mathbb{X}_1^L)^T \mathbb{X}_1^R (\mathbb{X}_1^L)^T \mathbb{X}_b^R$ is the MPO equal to the horizontal layer of impurities $\mathbb{X}_b^{L,R}$ in the same figure. The numerical procedure was applied in the following examples.

A. Toric code

The impurity projectors \tilde{P}_{\pm} together with IMPO fusion rules (23) determine the coefficients $\tilde{s}_{\pm 1} = 1/2$ and $\tilde{s}_{\pm 2} = \pm 1/2$. As for vertical projectors, the truncated sum runs over $b = 1$ only with degeneracy $G_1 = 1$. The topological entropies are

$$\tilde{\gamma}_{\pm} = \log 2X_{1,1}^a = \log 2 \quad (46)$$

within numerical precision. This number is obtained after numerical evaluation of the form factors and is consistent with the identification $\tilde{P}_+ = \tilde{P}_m$ and $\tilde{P}_- = \tilde{P}_e$.

B. Fibonacci string net

Numerical evaluation of coefficients \tilde{s}_b^a and the form factors yields

$$\tilde{\gamma}_1 = \log \frac{\mathcal{D}}{d_{\tau}}, \quad \tilde{\gamma}_2 = \log \frac{\mathcal{D}}{d_{\bar{\tau}}}, \quad \gamma_- = \log \frac{\mathcal{D}}{d_{\tau} d_{\bar{\tau}}} \quad (47)$$

with numerical precision. Here $\mathcal{D} = 2 + \phi$ is the total quantum dimension and $d_{\tau} = d_{\bar{\tau}} = \phi$. These numbers are consistent with the identifications: $\tilde{P}_1 = \tilde{P}_{\tau}$, $\tilde{P}_2 = \tilde{P}_{\bar{\tau}}$, and $\tilde{P}_3 = \tilde{P}_{\tau\bar{\tau}}$.

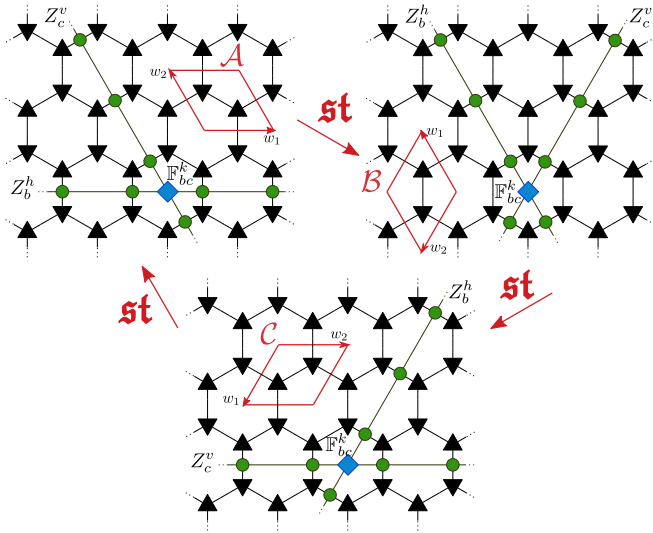


FIG. 5. Basic state. The object \mathbb{F}_{bc}^k , includes the lines of Z_b^h and Z_c^v and a tensor at their intersection. When $b = 1$ ($c = 1$) then \mathbb{F} is just vertical MPO symmetry Z_c^v (horizontal Z_b^h). When $b > 1$ then \mathbb{F}_{bc}^k is one of the IMPO symmetries. Inserted into an iPEPS wrapped on an infinite torus it yields state $|\mathbb{F}_{bc}^k\rangle$. The same set of states (for each b, c, k) can be found on each of the tori related by modular st transformation, where $(st)^3 = \mathbb{I}$, which corresponds to 120° counterclockwise rotation on the honeycomb lattice with the chosen tori defined by a pair of unit vectors (w_1, w_2) .

C. Ising string net

Similar numerical evaluation as for Fibonacci model yields

$$\tilde{\gamma}_\sigma = \log \frac{\mathcal{D}}{d_\sigma}, \quad \tilde{\gamma}_{\bar{\sigma}} = \log \frac{\mathcal{D}}{d_{\bar{\sigma}}}, \quad (48)$$

$$\tilde{\gamma}_{\sigma\bar{\psi}} = \log \frac{\mathcal{D}}{d_\sigma d_{\bar{\psi}}}, \quad \tilde{\gamma}_{\psi\bar{\sigma}} = \log \frac{\mathcal{D}}{d_\psi d_{\bar{\sigma}}}, \quad (49)$$

$$\tilde{\gamma}_\psi = \log \frac{\mathcal{D}}{d_\psi}, \quad \tilde{\gamma}_{\bar{\psi}} = \log \frac{\mathcal{D}}{d_{\bar{\psi}}}, \quad (50)$$

$$\tilde{\gamma}_{\sigma\bar{\sigma}} = \log \frac{\mathcal{D}}{d_\sigma d_{\bar{\sigma}}} \quad (51)$$

within numerical precision. Here the total quantum dimension is $\mathcal{D} = 4$ while $d_\sigma = d_{\bar{\sigma}} = \sqrt{2}$ and $d_\psi = d_{\bar{\psi}} = 1$. The numbers are consistent with the anticipated identification of the projectors.

VIII. TOPOLOGICAL S AND T MATRICES

For pedagogical reasons, up to this point we distinguished between vertical projectors, with a trivial $Z_1^h = 1^h$, and impurity projectors. For the present purpose of calculating topological S and T matrices it may be more convenient to treat them all on equal footing. We number MPO symmetries as $Z_a^{h,v}$ with $a = 1, \dots, n$, where $a = 1$ labels the trivial identities $1^{h,v}$. A basic building block for the projectors is \mathbb{F}_{bc}^k , shown in Fig. 5, including the lines of Z_b^h and Z_c^v and a tensor at their intersection. When $b = 1$ ($c = 1$) then \mathbb{F} is just vertical MPO symmetry Z_c^v (horizontal Z_b^h). When $b > 1$ then \mathbb{F}_{bc}^k is one of the IMPO symmetries. Therefore, in this unified

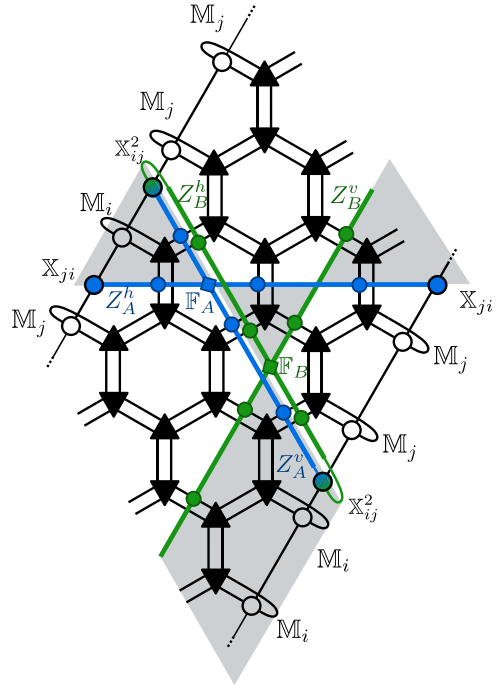


FIG. 6. The overlap in Eq. (55) between iPEPS' on infinite tori \mathcal{A} and \mathcal{B} calculated on torus \mathcal{B} , using its vertical boundary MPS. It involves a new class of impurity transfer matrices and their eigenvectors, where a nontrivial MPO symmetry is in only one layer of the PEPS (either bra or ket) or there are two nontrivial MPO symmetries in both layers but they are of a different type. Inserting an MPO symmetry may in general change the boundaries, hence the change of indices $\mathbb{M}_i \rightarrow \mathbb{M}_j$ and the gray shaded regions denoting these sector changes.

notation each (vertical or impurity) projector on anyon flux a can be expressed as a linear combination

$$P_a = \sum_{bc} \sum_k c_{kbc}^a \mathbb{F}_{bc}^k, \quad (52)$$

where the range of k depends on bc . When inserted into iPEPS wrapped on an infinite torus, the projector yields the ground state with anyon flux a in the horizontal direction:

$$|\Psi^a\rangle = \sum_{ab} \sum_k c_{kab}^a |\mathbb{F}_{ab}^k\rangle. \quad (53)$$

Here the last ket is the iPEPS inserted with $\mathbb{F}_{\alpha\beta}^k$. Up to this point there is nothing essentially new in this paragraph except for fixing notation.

States $|\Psi^a\rangle$ are used to calculate topological S and T matrices. Diagonal T matrix encodes self-statistics, while S matrix stands for mutual statistics. Together they form a representation of a modular group $SL(2, \mathbb{Z})$, by which they are related to the modular transformations of a torus generated by s and t transformations [61]. It follows that the matrix elements of a combination of the topological S and T matrices are given by the overlaps between $|\Psi^a\rangle$ transformed by a combination of corresponding modular matrices s and t .

Here we work with states on a hexagonal lattice with 120° rotational symmetry and we start by defining torus \mathcal{A} in Fig. 5 with unit vectors w_1, w_2 and corresponding transfer

matrices: vertical ($w_1, L_v w_2$) and horizontal ($L_h w_1, w_2$) with $L_{h,v} \rightarrow \infty$, see Fig. 2(b) for comparison. Next, we consider all transformations of the unit cell by st matrix, which generates 120° counterclockwise rotation, see Fig. 5. This results in tori \mathcal{B} and \mathcal{C} together with their corresponding transfer matrices as shown in Fig. 5. This construction, however, is general and can be applied to lattices with other symmetries as well.

Our method requires finding three complete sets of ground states

$$\{|\Psi_{\mathcal{A}}^a\rangle\}, \quad \{|\Psi_{\mathcal{B}}^a\rangle\}, \quad \{|\Psi_{\mathcal{C}}^a\rangle\}, \quad (54)$$

with well-defined anyon fluxes corresponding to three different tori: $\mathcal{A}, \mathcal{B}, \mathcal{C}$. Topological S and T matrices are extracted from all possible overlaps between states in (54). This algorithm is presented in Ref. [62] and slightly generalized in the Appendix of Ref. [48].

The core of the calculation is an overlap

$$\langle (\mathbb{F}_{ab}^k)_{\mathcal{A}} | (\mathbb{F}_{a'b'}^k)_{\mathcal{B}} \rangle, \quad (55)$$

shown in Fig. 6, between two iPEPS's on infinite tori \mathcal{A} and \mathcal{B} . It involves a new class of impurity transfer matrices and their eigenvectors, where a nontrivial MPO symmetry is in only one layer of the PEPS (either bra or ket) or there are two nontrivial MPO symmetries in both layers but they are of a different type. This type of overlap was encountered already in the Abelian case in Ref. [48] where they are explained in more detail. In the Abelian case the nontrivial MPO symmetry inserted in just one layer of the PEPS changes the boundary MPS $|v_i\rangle \rightarrow |v_j\rangle$, where $i \neq j$. However in the non-Abelian

case, all changes of the boundary MPS have to be considered including $i = j$. The possible change of the boundary conditions is denoted in Fig. 6 by shaded gray regions. Once the overlaps are found, we follow the algebra in Appendix B of Ref. [48] to obtain the following topological matrices S and T .

A. Toric code

For analytic tensors with $D = 4$ we obtain the exact matrices up to numerical precision:

$$S_{\text{TC}} = \frac{1}{2} \begin{pmatrix} 1 & 1 & 1 & 1 \\ 1 & 1 & -1 & -1 \\ 1 & -1 & 1 & -1 \\ 1 & -1 & -1 & 1 \end{pmatrix},$$

$$T_{\text{TC}} = \begin{pmatrix} 1 & 0 & 0 & 0 \\ 0 & 1 & 0 & 0 \\ 0 & 0 & 1 & 0 \\ 0 & 0 & 0 & -1 \end{pmatrix}.$$

Here consecutive columns and rows correspond to projectors that were labeled as $1, e, m, \epsilon$. These matrices confirm correctness of this labeling up to possible interchange of e and m that is a matter of convention.

B. Fibonacci string net

For the five states obtained with projectors $P_{\text{vac}}, P_{\tau\bar{\tau}}, \tilde{P}_{\tau\bar{\tau}}, \tilde{P}_{\tau}, \tilde{P}_{\bar{\tau}}$ we obtain the matrices:

$$S_{\text{Fib}} = \frac{1}{D} \begin{pmatrix} 1 & \varphi^2 & \varphi^2 & \varphi & \varphi \\ \varphi^2 & 1 & 1 & -\varphi & -\varphi \\ \varphi^2 & 1 & 1 & -\varphi & -\varphi \\ \varphi & -\varphi & -\varphi & -1 & \varphi^2 \\ \varphi & -\varphi & -\varphi & \varphi^2 & -1 \end{pmatrix}, \quad T_{\text{Fib}} = \begin{pmatrix} 1 & 0 & 0 & 0 & 0 \\ 0 & 1 & 0 & 0 & 0 \\ 0 & 0 & 1 & 0 & 0 \\ 0 & 0 & 0 & e^{4i\pi/5} & 0 \\ 0 & 0 & 0 & 0 & e^{-4i\pi/5} \end{pmatrix}.$$

For brevity matrix S_{Fib} is shown exact with $\varphi = d_\tau = \frac{1}{2}(1 + \sqrt{5})$ although we obtain it with numerical accuracy $\mathcal{O}(10^{-10})$. It is clear that we can remove either second or third row and column because they both correspond to two equivalent ways of obtaining flux $\tau\bar{\tau}$.

C. Ising string net

For the ten states obtained with projectors $P_{\text{vac}}, P_{\psi\bar{\psi}}, P_{\sigma\bar{\sigma}}, \tilde{P}_{\sigma\bar{\sigma}}, \tilde{P}_{\psi\bar{\psi}}, \tilde{P}_{\psi}, \tilde{P}_{\sigma}, \tilde{P}_{\sigma\bar{\psi}}, \tilde{P}_{\bar{\sigma}}, \tilde{P}_{\psi\bar{\sigma}}$ we obtain the matrices with numerical accuracy $\mathcal{O}(10^{-13})$:

$$S_{\text{Is}} = \frac{1}{4} \begin{pmatrix} 1 & 1 & 2 & 2 & 1 & 1 & \sqrt{2} & \sqrt{2} & \sqrt{2} & \sqrt{2} \\ 1 & 1 & 2 & 2 & 1 & 1 & -\sqrt{2} & -\sqrt{2} & -\sqrt{2} & -\sqrt{2} \\ 2 & 2 & 0 & 0 & -2 & -2 & 0 & 0 & 0 & 0 \\ 2 & 2 & 0 & 0 & -2 & -2 & 0 & 0 & 0 & 0 \\ 1 & 1 & -2 & -2 & 1 & 1 & \sqrt{2} & \sqrt{2} & -\sqrt{2} & -\sqrt{2} \\ 1 & 1 & -2 & -2 & 1 & 1 & -\sqrt{2} & -\sqrt{2} & \sqrt{2} & \sqrt{2} \\ \sqrt{2} & -\sqrt{2} & 0 & 0 & \sqrt{2} & -\sqrt{2} & 0 & 0 & 2 & -2 \\ \sqrt{2} & -\sqrt{2} & 0 & 0 & \sqrt{2} & -\sqrt{2} & 0 & 0 & -2 & 2 \\ \sqrt{2} & -\sqrt{2} & 0 & 0 & -\sqrt{2} & \sqrt{2} & 2 & -2 & 0 & 0 \\ \sqrt{2} & -\sqrt{2} & 0 & 0 & -\sqrt{2} & \sqrt{2} & -2 & 2 & 0 & 0 \end{pmatrix},$$

$$T_{\text{Is}} = \begin{pmatrix} 1 & 0 & 0 & 0 & 0 & 0 & 0 & 0 & 0 & 0 & 0 \\ 0 & 1 & 0 & 0 & 0 & 0 & 0 & 0 & 0 & 0 & 0 \\ 0 & 0 & 1 & 0 & 0 & 0 & 0 & 0 & 0 & 0 & 0 \\ 0 & 0 & 0 & 1 & 0 & 0 & 0 & 0 & 0 & 0 & 0 \\ 0 & 0 & 0 & 0 & -1 & 0 & 0 & 0 & 0 & 0 & 0 \\ 0 & 0 & 0 & 0 & 0 & -1 & 0 & 0 & 0 & 0 & 0 \\ 0 & 0 & 0 & 0 & 0 & 0 & 0 & e^{i\pi/8} & 0 & 0 & 0 \\ 0 & 0 & 0 & 0 & 0 & 0 & 0 & 0 & -e^{i\pi/8} & 0 & 0 \\ 0 & 0 & 0 & 0 & 0 & 0 & 0 & 0 & 0 & e^{-i\pi/8} & 0 \\ 0 & 0 & 0 & 0 & 0 & 0 & 0 & 0 & 0 & 0 & -e^{-i\pi/8} \end{pmatrix}.$$

It is clear that we can remove either the third or fourth row and column because they both correspond to two equivalent ways of obtaining flux $\sigma\bar{\sigma}$.

IX. SUMMARY

We presented numerical method to determine non-Abelian topological order in iPEPS representing the unique ground state on infinite two-dimensional lattice. The method is based on finding consecutively the following elements:

(1) All of the boundary fixed points of PEPS transfer matrices in the form of matrix product operators v_i ;

(2) All MPO symmetries Z_a mapping between the boundaries and their fusion rules;

(3) All impurity eigenvectors x_a of vertical impurity transfer matrices of PEPS inserted with horizontal MPO symmetries Z^h ;

(4) All impurity MPO symmetries \tilde{Z} mapping between the impurity eigenvectors;

(5) All projectors on states with well defined anyon flux along horizontal direction. They are linear combinations of either vertical MPO symmetries or vertical impurity MPO symmetries: $P_a = \sum_{bc} \sum_k c_{kbc}^a \mathbb{F}_{bc}^k$;

(6) All overlaps between states with definite anyon flux on different infinite tori related by modular transformations.

The topological charges and mutual statistics in the form of topological S and T matrices are recovered from the overlaps. They provide full topological characterization of string net models.

A byproduct of the linear ansatz for a projector is an efficient algorithm to obtain the second Renyi topological entanglement entropy directly in the thermodynamic limit. In addition to tests for the string net models, we found nonzero TEE in the variational ansatz of Ref. [46] for the Kitaev model in magnetic field [3], see Appendix E.

ACKNOWLEDGMENTS

We are indebted to Lukasz Cincio and Guifre Vidal, the coauthors of our common Ref. [48], for laying foundations for the present generalization. Special thanks to Lukasz for helpful comments on the present paper. We would also like to thank Hyun-Yong Lee for very useful feedback on the ansatz in Ref. [46]. A.F. would like to thank Bram Vanhecke for explaining the VUMPS algorithm. Numerical calculations were performed in MATLAB with the help of `ncon` function [63] for tensor contractions. A.F. acknowledges financial support by Polish Ministry of Science and Education, Project No.

DI2015 021345, from the budget funds for science in 2016–2020 under the Diamond Grant program. This research was supported by Narodowe Centrum Nauki (NCN) under Grant No. 2019/35/B/ST3/01028 (A.F., J.D.) and Etiuda Grant No. 2020/36/T/ST3/00451 (A.F.).

APPENDIX A: FUSION RULES

Fusion rules are encoded in F symbols which have to satisfy the Pentagon equation:

$$\begin{array}{c} a \quad \quad \quad d \\ \diagdown \quad \diagup \\ \quad e \quad \quad \\ \diagup \quad \diagdown \\ b \quad \quad \quad c \end{array} = F_{def}^{abc} \begin{array}{c} a \quad \quad \quad d \\ \diagdown \quad \diagup \\ \quad f \quad \quad \\ \diagup \quad \diagdown \\ b \quad \quad \quad c \end{array}$$

F symbols of both non-Abelian models are mostly given by the allowed fusions: N_{ab}^c describing $a \times b \rightarrow c$ with all its (allowed) permutations:

(i) for Fibonacci: $N_{11}^1 = N_{\tau\tau}^1 = N_{\tau\tau}^\tau = 1$

(ii) for Ising: $N_{11}^1 = N_{\sigma\sigma}^1 = N_{\psi\psi}^1 = N_{\psi\psi}^\sigma = 1$.

Then $F_{def}^{abc} = N_{ab}^e N_{cd}^f N_{ad}^f N_{bc}^e$ unless they are overwritten by additional special rules:

(i) for Fibonacci: $F_{\tau 11}^{\tau\tau\tau} = -F_{\tau\tau\tau}^{\tau\tau\tau} = \frac{1}{d_\tau}$ and $F_{\tau\tau 1}^{\tau\tau\tau} = \frac{1}{\sqrt{d_\tau}}$.

(ii) for Ising: $F_{\sigma 11}^{\sigma\sigma\sigma} = F_{\sigma 1\psi}^{\sigma\sigma\sigma} = F_{\sigma\psi 1}^{\sigma\sigma\sigma} = -F_{\sigma\psi\psi}^{\sigma\sigma\sigma} = \frac{1}{\sqrt{2}}$ and $F_{\sigma\sigma\sigma}^{\psi\sigma\psi} = F_{\psi\sigma\sigma}^{\psi\sigma\psi} = -1$.

APPENDIX B: iPEPS TENSORS

iPEPS tensors, shown in Fig. 7, are given by the following combination of F symbols and quantum dimensions d_i :

$$A_{\alpha\beta\gamma}^i = \left(\frac{d_a d_b}{d_c}\right)^{1/4} F_{fec}^{dab} \delta_{aa'} \delta_{bb'} \delta_{cc'} \delta_{dd'} \delta_{ee'} \delta_{ff'} \quad (\text{B1})$$

$$B_{\alpha\beta\gamma}^i = \left(\frac{d_a d_b}{d_c}\right)^{1/4} F_{fec}^{dab} \delta_{aa'} \delta_{bb'} \delta_{cc'} \delta_{dd'} \delta_{ee'} \delta_{ff'}. \quad (\text{B2})$$

By construction each tensor has a triple of bond indices along each of the three bonds towards NN lattice sites. We concatenate each triple into a single bond index, e.g., $\alpha = (a, e, d')$. The physical index is also a triple index $i = (a', b', c')$. These basic tensors are forming the topological state after proper contraction of bond indices with respect to their triplet structure. For the toric code and double Fibonacci string nets the bond dimension $D = 2^3 = 8$ is redundantly large and can be reduced to $D = 4$ and $D = 5$ after applying projectors on the bond indices, namely the only nonzero

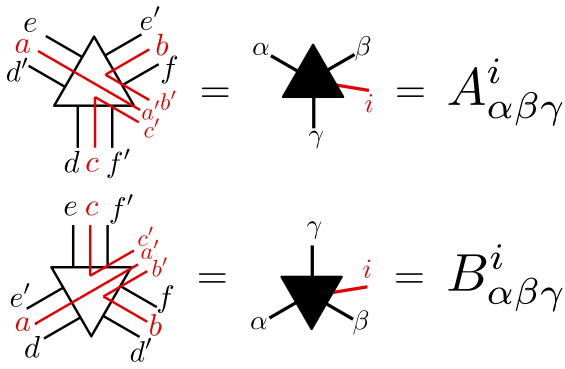


FIG. 7. Tensors forming the iPEPS are defined via combination of F -symbols and corresponding quantum dimensions d_i . All bond indices and the physical index are in fact a triple index. The bond dimension can be reduced by applying projectors on the non zero bond indices.

combinations of bond indices (i, j, k) are those in which the fusion product $i \times j \times k = 1 + \dots$ contains the trivial anyon. For the double Ising string net, on the other hand, the original bond dimension $D = 3^3 = 27$ can be reduced to $D = 10$.

APPENDIX C: PERTURBATION OF TENSOR SYMMETRY

In Ref. [48] we demonstrated that with our method it is possible to obtain accurate results for topological S and T matrices from a numerically optimized iPEPS ground state of the Kitaev honeycomb model for a wide range of coupling parameters. In the case of Fibonacci and Ising string nets, whose parent Hamiltonians are far more complex, the same test would go far beyond the scope of the present paper.

$$S_{\text{Fib}} = \begin{pmatrix} 0.2771 & 0.7251 & 0.7252 & 0.4484 & 0.4484 \\ 0.7251 & 0.2735 & 0.2749 & -0.4486 & -0.4486 \\ 0.7252 & 0.2749 & 0.2764 & -0.4472 & -0.4472 \\ 0.4484 & -0.4486 & -0.4472 & -0.2764 & 0.7236 \\ 0.4484 & -0.4486 & -0.4472 & 0.7236 & -0.2764 \end{pmatrix}$$

and

$$\text{diag}(T_{\text{Fib}}) = \begin{pmatrix} 1.0000 - 0.0000i \\ 1.0000 + 0.0000i \\ 1.0000 - 0.0000i \\ -0.8090 - 0.5878i \\ -0.8090 + 0.5878i \end{pmatrix}.$$

When compared to the exact numbers, their maximal error is of the order of 10^{-3} . Although there are four anyon fluxes in the Fibonacci model, here as in the main text we keep both $\mathcal{P}_{\tau\bar{\tau}}$ and $\tilde{\mathcal{P}}_{\tau\bar{\tau}}$ which project on the same flux $\tau\bar{\tau}$.

For the Ising string-net model we added a perturbation shown in Fig. 8 with strength $\epsilon = 0.5$, which lead to even more accurate results. We obtained topological entanglement entropy and topological S and T matrices with accuracy $\mathcal{O}(10^{-6})$.

In order to complete the discussion about random perturbations that may arise during numerical optimization of iPEPS

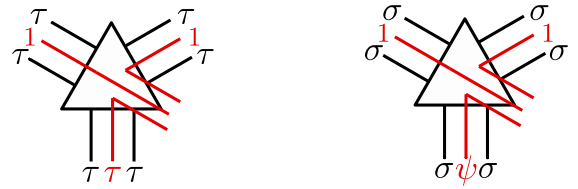


FIG. 8. Symmetry breaking perturbations in Fibonacci (left) and Ising (right) string nets.

However, as most concerns about stability arise from Ref. [64], we can introduce their perturbation at the virtual level of the tensor network—which violates the exact MPO symmetries—to see how our algorithm performs under this crash test.

The vertex violating terms [64], T_p , which are allowed in the stand-alone space but do not represent the physical ground state, are shown in Fig. 8. Additionally we allow all three rotations of the red indices. The fixed-point tensors T are perturbed by adding a vertex violating term T_p controlled by a small parameter ϵ :

$$T \rightarrow T + \epsilon T_p. \quad (\text{C1})$$

For the Fibonacci string-net model perturbed with a strong $\epsilon = 0.1$ we obtained the following topological entanglement entropies:

$$\begin{pmatrix} 1.2847 \\ 0.3235 \\ 0.3235 \\ 0.8047 \\ 0.8047 \end{pmatrix}, \quad (\text{C2})$$

and the following topological matrices:

we calculated the topological data for a completely random, real perturbation in the Fibonacci string-net model:

$$T \rightarrow T + \epsilon T_{\text{random}}. \quad (\text{C3})$$

For $\epsilon = 0.01$ we recovered the topological entanglement entropies and topological matrices with accuracy of the order of $\mathcal{O}(10^{-4})$.

APPENDIX D: INTRODUCING FINITE CORRELATION LENGTH

In order to see how the algorithm performs when the iPEPS tensors are driven away from the fixed point by introducing a finite correlation length, we apply the local filtering introduced in Refs. [65–67] to the fixed point of the Fibonacci string-net model. The perturbation has the following form:

$$|\Psi\rangle \rightarrow \prod_i e^{\beta\sigma_i} |\Psi\rangle, \quad (\text{D1})$$

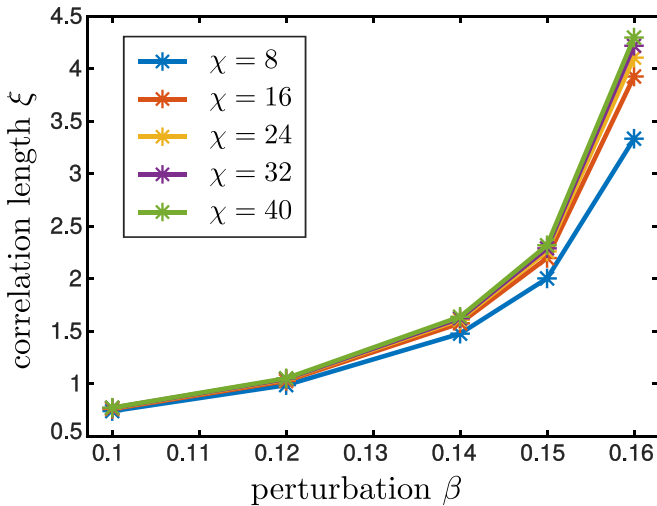


FIG. 9. The correlation length ξ in the Fibonacci string net model in function of the perturbation parameter β in Eq. (D1). Different colors correspond to different bond dimensions χ of the boundary MPS v_i .

where the index i runs over all physical indices and σ^z is the third Pauli matrix. In Ref. [48], by considering a similar perturbation to the toric code, we demonstrated that with our algorithm it is possible to obtain topological S and T matrices for states with correlation length much longer than achievable by the state of the art 2D DMRG techniques.

Figure 9 shows how the correlation length grows with parameter β for the perturbed Fibonacci string-net model. In the Fibonacci model, for parameters $\beta = 0.14, 0.15, 0.16$ such that the correlation length $\xi > 1$, we obtained the topological entanglement entropies and the topological S and T matrices. Their maximal errors are listed in Table I.

APPENDIX E: VARIATIONAL ANSATZ FOR THE KITAEV MODEL IN (1,1,1) MAGNETIC FIELD

We investigate the ansatz proposed in the Supplemental Material of Ref. [46]. Although it satisfies all desired

TABLE I. For different values of the perturbation parameter β in Eq. (D1), the table lists corresponding correlation lengths, ξ , and maximal errors of the entries of the list of topological entanglement entropies, ϵ_γ , and the S and T matrices, ϵ_S and ϵ_T .

| β | ξ | ϵ_γ | ϵ_S | ϵ_T |
|---------|-------|-------------------------|-------------------------|-------------------------|
| 0 | 0 | $\mathcal{O}(10^{-10})$ | $\mathcal{O}(10^{-10})$ | $\mathcal{O}(10^{-10})$ |
| 0.14 | 1.64 | $\mathcal{O}(10^{-3})$ | $\mathcal{O}(10^{-4})$ | $\mathcal{O}(10^{-6})$ |
| 0.15 | 2.32 | $\mathcal{O}(10^{-2})$ | $\mathcal{O}(10^{-3})$ | $\mathcal{O}(10^{-7})$ |
| 0.16 | 4.3 | $\mathcal{O}(10^{-2})$ | $\mathcal{O}(10^{-3})$ | $\mathcal{O}(10^{-4})$ |

symmetries and has competitive energy, the ansatz was not demonstrated to possess the expected chiral Ising universality class [3]. We show that at least it has nontrivial topological entanglement entropy.

Each TM has two boundary fixed points. They have large bond dimension χ necessary to accommodate a long correlation length. For $\chi = 150$ the correlation length saturates at $\xi \simeq 15.4$. However, when it comes to calculating the topological entanglement entropy, whose cost is much steeper in χ , we will be satisfied with $\chi = 50$, corresponding to $\xi \simeq 10.3$, that is sufficient to recover exact symmetries. There is one nontrivial \mathcal{Z}_2 symmetry such that $v_1^L \cdot Z_2^v = v_2^L$ and $v_2^L \cdot Z_2^v = v_1^L$ and, consequently,

$$Z_2^v \cdot Z_2^v = 1^v. \quad (\text{E1})$$

This is the algebra of the \mathcal{Z}_2 gauge field that was implemented in the ansatz by construction.

Like in the toric code, the \mathcal{Z}_2 algebra (E1) allows for two vertical projectors:

$$P_\pm = \frac{1}{2}(1^v \pm Z^v). \quad (\text{E2})$$

They project on ± 1 horizontal flux of the \mathcal{Z}_2 gauge field, see Ref. [46]. In this model, when the horizontal cylinder is closed into a torus, the vertical flux also becomes a good quantum number. For an iPEPS wrapped on a torus (without horizontal line Z_2^h) the state is a superposition of both ± 1 vertical fluxes with equal amplitudes.

We also find nontrivial IMPO symmetry \tilde{Z}_2^v satisfying the \mathcal{Z}_2 algebra. It allows for two projectors:

$$\tilde{P}_\pm = \frac{1}{2}(\tilde{1}^v \pm \tilde{Z}_2^v). \quad (\text{E3})$$

Like the vertical projectors, they project on ± 1 horizontal flux of the \mathcal{Z}_2 gauge field but with a superposition of vertical fluxes with opposite amplitudes. Therefore, unlike the Fibonacci and Ising string net, neither of these two impurity projectors can be identified with any of the two vertical projectors P_\pm .

For vertical projectors we obtain topological entanglement entropy

$$\gamma_\pm = \log 2 \quad (\text{E4})$$

in the vacuum and vortex sector, respectively. This demonstrates topological order in the variational iPEPS of Ref. [46]. The impurity projectors also yield

$$\tilde{\gamma}_\pm = \log 2 \quad (\text{E5})$$

but here the minimally entangled states \pm are different combinations of the vertical \mathcal{Z}_2 flux than in Eq. (E4).

- [1] X. G. Wen, Topological orders in rigid states, *Int. J. Mod. Phys. B* **4**, 239 (1990).
- [2] A. Kitaev, Fault-tolerant quantum computation by anyons, *Ann. Phys.* **303**, 2 (2003).
- [3] A. Kitaev, Anyons in an exactly solved model and beyond, *Ann. Phys.* **321**, 2 (2006).
- [4] M. A. Levin and X.-G. Wen, String-net condensation: A physical mechanism for topological phases, *Phys. Rev. B* **71**, 045110 (2005).
- [5] Y. Kasahara, T. Ohnishi, Y. Mizukami, O. Tanaka, S. Ma, K. Sugii, N. Kurita, H. Tanaka, J. Nasu, Y. Motome, T. Shibauchi, and Y. Matsuda, Majorana quantization and half-integer thermal quantum Hall effect in a Kitaev spin liquid, *Nature (London)* **559**, 227 (2018).
- [6] S. R. White, Density Matrix Formulation for Quantum Renormalization Groups, *Phys. Rev. Lett.* **69**, 2863 (1992).
- [7] S. R. White, Density-matrix algorithms for quantum renormalization groups, *Phys. Rev. B* **48**, 10345 (1993).
- [8] S. Yan, D. A. Huse, and S. R. White, Spin-liquid ground state of the $S = 1/2$ Kagome Heisenberg antiferromagnet, *Science* **332**, 1173 (2011).
- [9] H.-C. Jiang, Z. Wang, and L. Balents, Identifying topological order by entanglement entropy, *Nat. Phys.* **8**, 902 (2012).
- [10] S.-S. Gong, D. N. Sheng, O. I. Motrunich, and M. P. A. Fisher, Phase diagram of the spin-1/2 $J_1 - J_2$ Heisenberg model on a honeycomb lattice, *Phys. Rev. B* **88**, 165138 (2013).
- [11] Z. Zhu, D. A. Huse, and S. R. White, Weak Plaquette Valence Bond Order in the $S = 1/2$ Honeycomb $J_1 - J_2$ Heisenberg Model, *Phys. Rev. Lett.* **110**, 127205 (2013).
- [12] S.-S. Gong, W. Zhu, and D. N. Sheng, Emergent chiral spin liquid: Fractional quantum Hall effect in a Kagome Heisenberg model, *Sci. Rep.* **4**, 6317 (2014).
- [13] Z. Zhu and S. R. White, Quantum phases of the frustrated XY models on the honeycomb lattice, *Mod. Phys. Lett. B* **28**, 1430016 (2014).
- [14] S.-S. Gong, W. Zhu, L. Balents, and D. N. Sheng, Global phase diagram of competing ordered and quantum spin-liquid phases on the kagome lattice, *Phys. Rev. B* **91**, 075112 (2015).
- [15] W.-J. Hu, S.-S. Gong, W. Zhu, and D. N. Sheng, Competing spin-liquid states in the spin-1/2 Heisenberg model on the triangular lattice, *Phys. Rev. B* **92**, 140403(R) (2015).
- [16] W. Zhu, S. S. Gong, D. N. Sheng, and L. Sheng, Possible non-Abelian Moore-Read state in double-layer bosonic fractional quantum Hall system, *Phys. Rev. B* **91**, 245126 (2015).
- [17] Z. Zhu and S. R. White, Spin liquid phase of the $S = 1/2$ $J_1 - J_2$ Heisenberg model on the triangular lattice, *Phys. Rev. B* **92**, 041105(R) (2015).
- [18] M. P. Zaletel, Z. Zhu, Y.-M. Lu, A. Vishwanath, and S. R. White, Space Group Symmetry Fractionalization in a Chiral Kagome Heisenberg Antiferromagnet, *Phys. Rev. Lett.* **116**, 197203 (2016).
- [19] T.-S. Zeng, W. Zhu, J.-X. Zhu, and D. N. Sheng, Nature of continuous phase transitions in interacting topological insulators, *Phys. Rev. B* **96**, 195118 (2017).
- [20] M.-S. Vaezi and A. Vaezi, Numerical observation of parafermion zero modes and their stability in 2D topological states, *arXiv:1706.01192*.
- [21] Z. Zhu, I. Kimchi, D. N. Sheng, and L. Fu, Robust non-Abelian spin liquid and a possible intermediate phase in the antiferromagnetic Kitaev model with magnetic field, *Phys. Rev. B* **97**, 241110(R) (2018).
- [22] M. Gohlke, G. Wachtel, Y. Yamaji, F. Pollmann, and Y. B. Kim, Quantum spin liquid signatures in Kitaev-like frustrated magnets, *Phys. Rev. B* **97**, 075126 (2018).
- [23] M. Gohlke, R. Moessner, and F. Pollmann, Dynamical and topological properties of the Kitaev model in a [111] magnetic field, *Phys. Rev. B* **98**, 014418 (2018).
- [24] L. Cincio and G. Vidal, Characterizing Topological Order by Studying the Ground States on an Infinite Cylinder, *Phys. Rev. Lett.* **110**, 067208 (2013).
- [25] Y.-C. He, D. N. Sheng, and Y. Chen, Chiral Spin Liquid in a Frustrated Anisotropic Kagome Heisenberg Model, *Phys. Rev. Lett.* **112**, 137202 (2014).
- [26] W. Zhu, S. S. Gong, F. D. M. Haldane, and D. N. Sheng, Topological characterization of the non-Abelian Moore-Read state using density-matrix renormalization group, *Phys. Rev. B* **92**, 165106 (2015).
- [27] W. Zhu, S. S. Gong, and D. N. Sheng, Chiral and critical spin liquids in a spin-1/2 kagome antiferromagnet, *Phys. Rev. B* **92**, 014424 (2015).
- [28] B. Bauer, L. Cincio, B. P. Keller, M. Dolfi, G. Vidal, S. Trebst, and A. W. W. Ludwig, Chiral spin liquid and emergent anyons in a Kagome lattice Mott insulator, *Nat. Commun.* **5**, 5137 (2014).
- [29] W. Zhu, S. S. Gong, F. D. M. Haldane, and D. N. Sheng, Fractional Quantum Hall States at $\nu = 13/5$ and $12/5$ and Their Non-Abelian Nature, *Phys. Rev. Lett.* **115**, 126805 (2015).
- [30] A. G. Grushin, J. Motruk, M. P. Zaletel, and F. Pollmann, Characterization and stability of a fermionic $\nu = 1/3$ fractional Chern insulator, *Phys. Rev. B* **91**, 035136 (2015).
- [31] Y.-C. He, S. Bhattacharjee, F. Pollmann, and R. Moessner, Kagome Chiral Spin Liquid as a Gauged $U(1)$ Symmetry Protected Topological Phase, *Phys. Rev. Lett.* **115**, 267209 (2015).
- [32] Y.-C. He and Y. Chen, Distinct Spin Liquids and Their Transitions in Spin-1/2 XXZ Kagome Antiferromagnets, *Phys. Rev. Lett.* **114**, 037201 (2015).
- [33] Y.-C. He, S. Bhattacharjee, R. Moessner, and F. Pollmann, Bosonic Integer Quantum Hall Effect in an Interacting Lattice Model, *Phys. Rev. Lett.* **115**, 116803 (2015).
- [34] S. Geraedts, M. P. Zaletel, Z. Papić, and R. S. K. Mong, Competing Abelian and non-Abelian topological orders in $\nu = 1/3 + 1/3$ quantum Hall bilayers, *Phys. Rev. B* **91**, 205139 (2015).
- [35] R. S. K. Mong, M. P. Zaletel, F. Pollmann, and Z. Papić, Fibonacci anyons and charge density order in the $12/5$ and $13/5$ quantum Hall plateaus, *Phys. Rev. B* **95**, 115136 (2017).
- [36] Y.-C. He, F. Grusdt, A. Kaufman, M. Greiner, and A. Vishwanath, Realizing and adiabatically preparing bosonic integer and fractional quantum Hall states in optical lattices, *Phys. Rev. B* **96**, 201103(R) (2017).
- [37] E. M. Stoudenmire, D. J. Clarke, R. S. K. Mong, and J. Alicea, Assembling Fibonacci anyons from a Z_3 parafermion lattice model, *Phys. Rev. B* **91**, 235112 (2015).
- [38] Y.-C. He, M. P. Zaletel, M. Oshikawa, and F. Pollmann, Signatures of Dirac Cones in a DMRG Study of the Kagome Heisenberg Model, *Phys. Rev. X* **7**, 031020 (2017).
- [39] S. N. Saadatmand and I. P. McCulloch, Symmetry fractionalization in the topological phase of the spin-1/2 $J_1 - J_2$

- triangular Heisenberg model, *Phys. Rev. B* **94**, 121111(R) (2016).
- [40] C. Hickey, L. Cincio, Z. Papić, and A. Paramekanti, Haldane-Hubbard Mott Insulator: From Tetrahedral Spin Crystal to Chiral Spin Liquid, *Phys. Rev. Lett.* **116**, 137202 (2016).
- [41] M. P. Zaletel, Y.-M. Lu, and A. Vishwanath, Measuring space-group symmetry fractionalization in Z_2 spin liquids, *Phys. Rev. B* **96**, 195164 (2017).
- [42] T.-S. Zeng, W. Zhu, and D. Sheng, Tuning topological phase and quantum anomalous Hall effect by interaction in quadratic band touching systems, *npj Quantum Mater.* **3**, 49 (2018).
- [43] F. Verstraete and J. I. Cirac, Renormalization algorithms for Quantum-Many Body Systems in two and higher dimensions, [arXiv:cond-mat/0407066](https://arxiv.org/abs/cond-mat/0407066).
- [44] V. Murg, F. Verstraete, and J. I. Cirac, Variational study of hardcore bosons in a two-dimensional optical lattice using projected entangled pair states, *Phys. Rev. A* **75**, 033605 (2007).
- [45] F. Verstraete, V. Murg, and J. I. Cirac, Matrix product states, projected entangled pair states, and variational renormalization group methods for quantum spin systems, *Adv. Phys.* **57**, 143 (2008).
- [46] H.-Y. Lee, R. Kaneko, T. Okubo, and N. Kawashima, Gapless Kitaev Spin Liquid to Classical String Gas Through Tensor Networks, *Phys. Rev. Lett.* **123**, 087203 (2019).
- [47] P. Corboz, Variational optimization with infinite projected entangled-pair states, *Phys. Rev. B* **94**, 035133 (2016).
- [48] A. Francuz, J. Dziarmaga, G. Vidal, and L. Cincio, Determining topological order from infinite projected entangled pair states, *Phys. Rev. B* **101**, 041108(R) (2020).
- [49] M. B. Şahinoğlu, D. Williamson, N. Bultinck, M. Mariën, J. Haegeman, N. Schuch, and F. Verstraete, Characterizing topological order with matrix product operators, [arXiv:1409.2150](https://arxiv.org/abs/1409.2150).
- [50] N. Bultinck, M. Mariën, D. J. Williamson, M. B. Şahinoğlu, J. Haegeman, and F. Verstraete, Anyons and matrix product operator algebras, *Ann. Phys.* **378**, 183 (2017).
- [51] M. Iqbal, K. Duivenvoorden, and N. Schuch, Study of anyon condensation and topological phase transitions from a Z_4 topological phase using the projected entangled pair states approach, *Phys. Rev. B* **97**, 195124 (2018).
- [52] C. Fernández-González, R. S. K. Mong, O. Landon-Cardinal, D. Pérez-García, and N. Schuch, Constructing topological models by symmetrization: A projected entangled pair states study, *Phys. Rev. B* **94**, 155106 (2016).
- [53] S. P. G. Crone and P. Corboz, Detecting a Z_2 topologically ordered phase from unbiased infinite projected entangled-pair state simulations, *Phys. Rev. B* **101**, 115143 (2020).
- [54] H. He, H. Moradi, and X.-G. Wen, Modular matrices as topological order parameter by a gauge-symmetry-preserved tensor renormalization approach, *Phys. Rev. B* **90**, 205114 (2014).
- [55] V. Zauner-Stauber, L. Vanderstraeten, M. T. Fishman, F. Verstraete, and J. Haegeman, Variational optimization algorithms for uniform matrix product states, *Phys. Rev. B* **97**, 045145 (2018).
- [56] M. T. Fishman, L. Vanderstraeten, V. Zauner-Stauber, J. Haegeman, and F. Verstraete, Faster methods for contracting infinite two-dimensional tensor networks, *Phys. Rev. B* **98**, 235148 (2018).
- [57] G. De las Cuevas, J. I. Cirac, N. Schuch, and D. Perez-Garcia, Irreducible forms of matrix product states: Theory and applications, *J. Math. Phys.* **58**, 121901 (2017).
- [58] A. Kitaev and J. Preskill, Topological Entanglement Entropy, *Phys. Rev. Lett.* **96**, 110404 (2006).
- [59] J. I. Cirac, D. Poilblanc, N. Schuch, and F. Verstraete, Entanglement spectrum and boundary theories with projected entangled-pair states, *Phys. Rev. B* **83**, 245134 (2011).
- [60] S. T. Flammia, A. Hamma, T. L. Hughes, and X.-G. Wen, Topological Entanglement Rényi Entropy and Reduced Density Matrix Structure, *Phys. Rev. Lett.* **103**, 261601 (2009).
- [61] X.-G. Wen, A theory of 2+1D bosonic topological orders, *Nat. Sci. Rev.* **3**, 68 (2015).
- [62] Y. Zhang, T. Grover, and A. Vishwanath, General procedure for determining braiding and statistics of anyons using entanglement interferometry, *Phys. Rev. B* **91**, 035127 (2015).
- [63] R. N. C. Pfeifer, G. Evenbly, S. Singh, and G. Vidal, NCON: A tensor network contractor for MATLAB, [arXiv:1402.0939](https://arxiv.org/abs/1402.0939).
- [64] S. K. Shukla, M. B. Şahinoğlu, F. Pollmann, and X. Chen, Boson condensation and instability in the tensor network representation of string-net states, *Phys. Rev. B* **98**, 125112 (2018).
- [65] J. Haegeman, K. Van Acoleyen, N. Schuch, J. I. Cirac, and F. Verstraete, Gauging Quantum States: From Global to Local Symmetries in Many-Body Systems, *Phys. Rev. X* **5**, 011024 (2015).
- [66] J. Haegeman, V. Zauner, N. Schuch, and F. Verstraete, Shadows of anyons and the entanglement structure of topological phases, *Nat. Commun.* **6**, 8284 (2015).
- [67] G.-Y. Zhu and G.-M. Zhang, Gapless Coulomb State Emerging from a Self-Dual Topological Tensor-Network State, *Phys. Rev. Lett.* **122**, 176401 (2019).